A R C H I V E S O F M E T A L L U R G Y A N D M A T E R I A L S
Volume 53 2008 Issue 1

A. KORNEVA [1]* M. BIEDA*, G. KORZNIKOWA** J. BONARSKI* K. SZTWIERTNIA*

CRYSTALLOGRAPHIC ORIENTATION EVALUATION OF THE σ AND α PHASES IN HARD MAGNETIC Fe-30%Cr-8%Co ALLOY SUBJECTED TO COMPLEX LOADING

ORIENTACJA KRYSTALOGRAFICZNA FAZ σ I α W TWARDYM MAGNETYCZNIE STOPIE Fe-30%Cr-8%Co PO ODKSZTAŁCENIU W ZMIENNYM STANIE OBCIĄŻEŃ

Severe plastic deformation by upsetting and torsion of the single α phase Fe-30%Cr-8%Co alloy caused the formation of gradient structure throughout the cross sections of sample as well as the precipitation of the intermetallic σ phase when deformed at 750, 800 and 850°C. The strongest precipitation of the σ phase occurred in the area of the highest deformation placed close to the mobile anvil (in the bottom part of the sample).

The crystallographic orientations of the tetragonal σ phase and cubic α phase in mezzo, macro and microscale were analyzed. Various techniques as X-ray diffraction, electron back-scattered diffraction (EBSD) in the scanning electron microscope (SEM) as well as convergent beam electron diffraction (CBED) in the transmission electron microscope (TEM) were used.

Keywords: hard magnetic alloy, severe plastic deformation, crystallographic orientation, pole figure (PF), inverse pole figure (IPF), X-ray diffraction, EBSD/SEM, CBED/TEM

Intensywne odkształcenie metodą spęczania i skręcania jednofazowego stopu α Fe-30%Cr-8%Co spowodowało tworzenie się gradientowej mikrostruktury na poprzecznych przekrojach próbek, jak również wydzielanie się międzymetalicznej fazy σ w próbkach odkształconych w temperaturach 750, 800 i 850°C. Maksymalne wydzielanie fazy σ obserwuje się w strefie największego odkształcenia po stronie ruchomego kowadła w dolnej część próbek.

Zanalizowano orientacje krystalograficzne tetragonalnej fazy σ i regularnej fazy α w skali mezo, makro i mikro. W pracy wykorzystano zróżnicowane techniki badawcze: analizę rentgenowską, dyfrakcję elektronów wstecznie rozproszonych (EBSD) oraz dyfrakcję elektronów w wiązce zbieżnej (CBED) odpowiednionio w skaningowym i transmisyjnym mikroskopie elektronowym.

1. Introduction

The Fe-30%Cr-8%Co alloy belongs to hard magnetic materials of the precipitation-hardening class [1]. A high manufacturability is the advantage of these alloys: they can be treated by cutting in the high coercive state and by forging, drawing, rolling in the α and $\alpha+\gamma$ states, allowing to obtain half-finished products in the form of bars, sheets and wires. Due to the hot pressure treatment it becomes possible to produce magnets of complicated shapes.

The initial state before magnetic treatment is the α solid state, obtained by quenching from temperatures 1100÷1350°C in the case of alloys with high content of Co (more than 14%) and by homogenization at low temperatures in the case of alloys with low content of Co [2].

The formation of high coercive state occurs during decomposition of the α solid solution into two coherent phases: magnetic α_1 phase rich in Fe, Co and paramagnetic α_2 phase rich in Cr. Such a modulated microstructure provides high magnetic properties [3], however leads to a sharp decrease of the material strength and plasticity [4]. It has been known that severe plastic deformation can improve mechanical properties due to the change of phase size and morphology [5, 6]. To achieve that, the severe plastic deformation by complex loading at high temperatures has usually been applied.

* INSTITUTE OF METALLURGY AND MATERIALS SCIENCE, POLISH ACADEMY OF SCIENCES, 30-059 KRAKÓW, 25 REYMONTA STR., POLAND
** INSTITUTE OF PROBLEMS OF METAL SUPERPLASTICITY, RUSSIAN ACADEMY OF SCIENCES, 39 KHALTURINA STR., UFA, 450001, BASHKORTOSTAN, RUSSIA
[1] ON LEAVE FROM THE INSTITUTE OF PROBLEMS OF METAL SUPERPLASTICITY, RUSSIAN ACADEMY OF SCIENCES, 39 KHALTURINA STR., UFA, 450001, BASHKORTOSTAN, RUSSIA

However, the conditions of deformation have led to the precipitation of an intermetallic σ phase.

The ongoing purpose of this work was to clarify certain peculiarities of the σ phase precipitation as well as to define the crystallographic orientations of the α and σ phases.

2. Material and experimental procedure

The chemical composition of examined alloy is presented in Table 1. The cast alloy was subjected to homogenization at 750°C to obtain a solid α solution. Cylindrical samples of 12 mm diameter and 10 mm height were cut off from the ingot. Severe plastic deformation was achieved on an appropriately modernized "Instron" machine, which ensured the conditions for superplastic deformation. In the paper, the deformation was achieved in two separate stages: upsetting and then torsion applied to the lower part of the sample (Fig. 1).

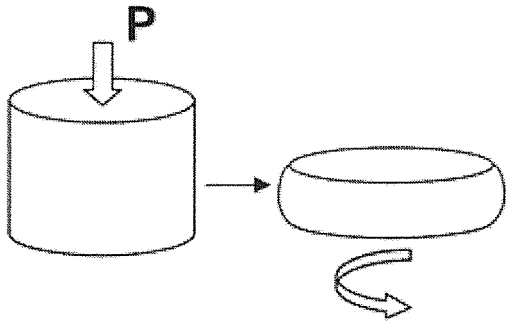

Fig. 1. The scheme of intense deformation by upsetting followed by torsion

TABLE 1

Chemical composition of the examined alloy

Cr	Co	Ti	V	Si	Fe
30	8	1	0.3	0.4	Remainder

The temperatures 750, 800, 850 and 900°C, were chosen for the deformation of the α phase. Samples were subjected to upsetting at the stain rate of $4 \cdot 10^{-4}$ s^{-1} to obtain the deformation of 40% followed by torsion at the strain rate of $8 \cdot 10^{-3}$ s^{-1} for up to 10 rotations. The above temperatures and deformation rates correspond to superplasticity conditions of the examined alloy.

The total degree of deformation was calculated based on the following formula (1) [7]:

$$\varepsilon = \varepsilon_1 + \varepsilon_2 = ln(h_0/h_{iR}) + ln(1 + (\varphi \cdot R/hiR)^2)^{1/2}, \quad (1)$$

where: ε_1 and ε_2 are the shares of upsetting and torsion in the deformation, respectively; φ is the rotation angle of the mobile anvil [rad]; R is the distance to the sample rotation axis; h_0 is the sample thickness before deformation; and h_{ik} is the sample thickness after deformation at distance R. The degree of deformation reached 0.5 and 3.5 (measured at half-distance to the rotation axis) by upsetting and torsion respectively.

The microstructure was examined by use of scanning (Jeol JXA 6400 and FEI XL 30 ESEM) and transmission electron microscopy (CM 20, Philips). The EBSD analysis was performed in the FEI SEM XL 30 ESEM. The CBED analysis was carried out using the Philips TEM CM 20, while X-ray diffraction analysis was done by the Philips PW1710 diffractometer using Cu $K\alpha$ radiation.

3. Results and discussion

3.1. Microstructure

The alloy Fe-30%Cr-8%Co revealed the single-phase microstructure of the α solid solution in the temperature range of annealing 750-900°C. The size of the α grains after annealing at 750, 800, 850 and 950°C were 40, 50, 70 and 300 μm, respectively. An example of microstructure after annealing at 800°C is presented in Fig. 2.

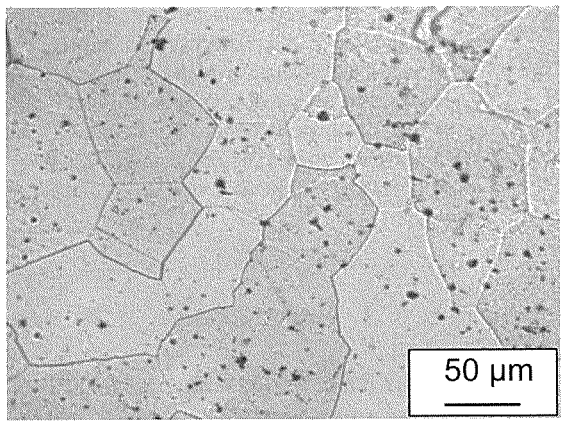

Fig. 2. Initial microstructure of the α solid solution after annealing at 800°C

The gradient microstructure was found in the cross-sections of deformed samples. Minimal grain size was observed at the bottom part of samples near the mobile anvil, where the highest deformation was achieved. Fig. 3 shows the panoramic image of cross section (a) and the detailed images of the microstructure at the top (b), middle (c) and bottom (d) parts of the sample deformed at 800°C. As it can be seen, apart from the refinement of the microstructure, precipitations of the second phase are appeared. The X-ray phase analysis identified them as the σ phase precipitates (Fig. 4).

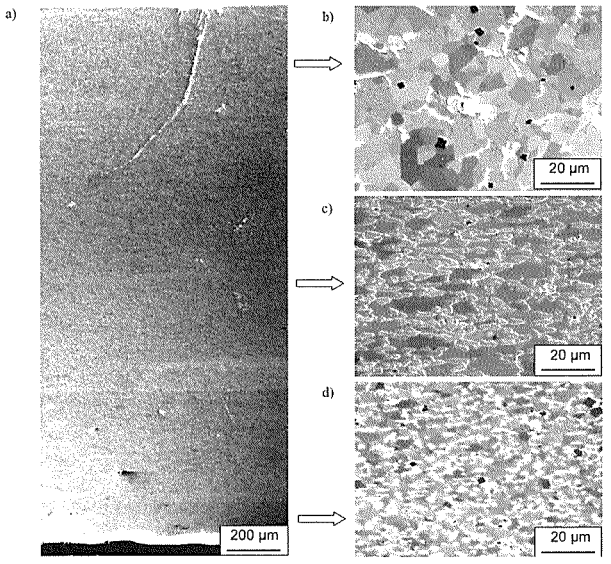

Fig. 3. Panoramic image of the cross sections (a) and detailed images of the microstructures in the top (b), middle (c) and bottom (d) areas of the sample deformed at 800°C

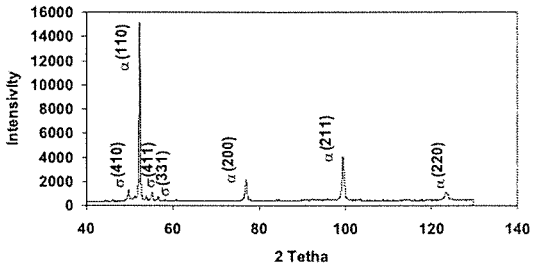

Fig. 4. X-ray analysis of the bottom area of the sample deformed at 800°C

Detailed microstructure analysis of all samples revealed another peculiarity of the σ phase precipitation. The σ phase precipitated along the grain boundary of the α phase which suggests that the precipitation of the σ phase was of a diffusional type. The maximum σ phase precipitation took place at the bottom of the samples where the maximal microstructure refinement was observed. Plausibly the processes of refinement of the α grains and the precipitation of the σ phase were affected by each other.

The maximal refinement of the microstructure and maximal precipitation of the σ phase were observed in the sample deformed at 800°C. The size of α and σ grains were about 3 and 2 µm, respectively.

3.2. Crystallographic orientations of the α phase in samples deformed at different temperatures. X-ray analysis

Longitudinal cross-sections from the bottom of samples deformed at 750, 800, 850 and 900°C were investigated. The position of the sample axis during the X-ray analysis is presented in Fig. 5.

Inverse pole figures (IPF), presented in Fig. 6, showed that crystallographic orientation distribution of the α grains for various temperatures was of the same type. In all cases the majority of the [213] and [114] directions was parallel to the Z axis.

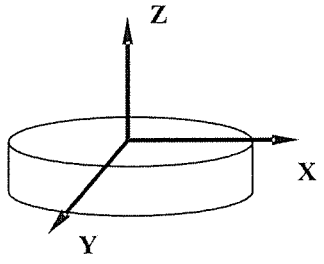

Fig. 5. Sample axis orientation during X-ray analysis and EBSD/SEM, CBED/TEM measurements

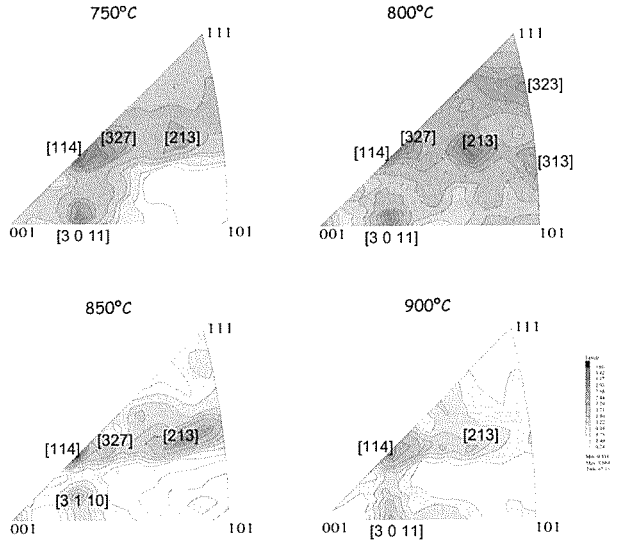

Fig. 6. Inverse pole figures of the α phase from the bottom of samples deformed at 750, 800, 850 and 900°C calculated from X-ray analysis

3.3. Crystallographic orientations of the α and σ phases in the sample deformed at 800°C. X-ray analysis

The longitudinal cross-section from the bottom of the sample deformed at 800°C was used for investigation.

Fig. 7 shows the pole figures (PFs) of the α and σ phases for (111) and (410) planes, respectively. It was found that the orientation distribution of the α grains was rather random, while texture of the σ grains was more prominent. The IPFs of the α and σ phases measured for Z direction are presented in Fig. 8. That made possible to define crystallographic directions of the α and σ phases

which were parallel to each other and to the deformation axis (Table 2).

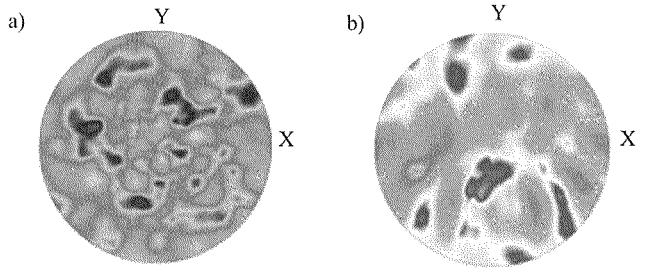

Fig. 7. Pole figures of the α (a) and σ (b) grains for {111} and {410} planes, respectively calculated from X-ray analysis

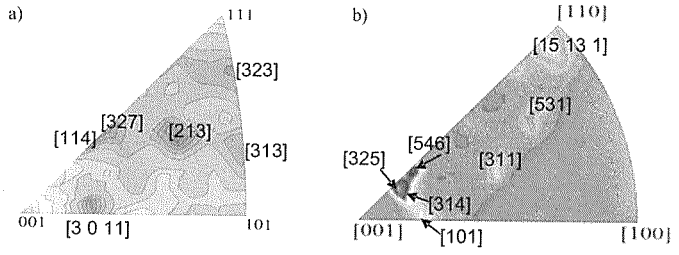

Fig. 8. Inverse pole figures of the α (a) and σ (b) grains for Z direction calculated from X-ray analysis

TABLE 2

Crystallographic directions of the α and σ phases which are parallel to each other and to deformation axis

Phase	Crystallographic directions
α phase	[114], [323], [213], [313], [3 0 11]
σ phase	[325], [546], [314], [101], [311], [531], [15 13 1]

3.4. Crystallographic orientations of the α and σ phases calculated from EBSD/SEM measurements

The same cross-section was analyzed by the use of EBSD/SEM. The scheme of sample axis orientation was the same as in the X-ray analysis. The phase map of the examined area ($6 \cdot 10^{-3}$ mm^2) is presented in Fig. 9.

Texture of the α phase was similar to the {100}<001> one rotated 45° anticlockwise around the Z axis and about 20° clockwise around the Y axis (Fig. 10a). Texture of the σ phase was weaker however not random and some peaks in the first and fourth quarter of the pole figure could be distinguished (Fig. 10b). The PF for sample deformed at 800°C shows the strongest component. It corresponds to the maximum refinement of the microstructure at this temperature.

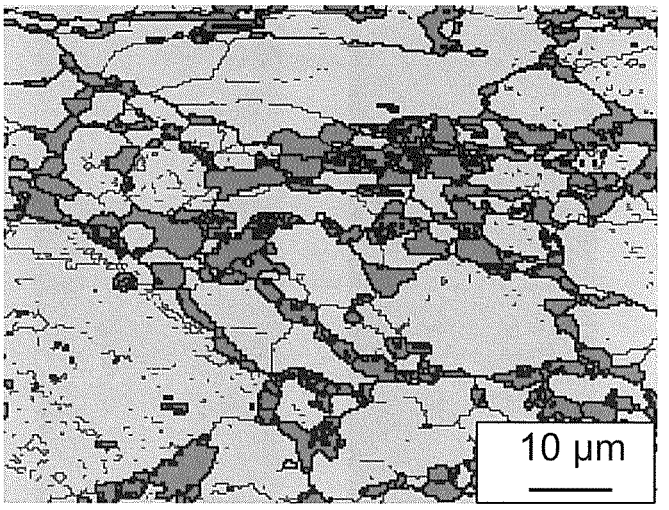

Fig. 9. Phase map of longitudinal section from the bottom of the sample deformed at 800°C, EBSD/SEM. Light grey color corresponds to the α phase, the dark grey color - to the σ phase

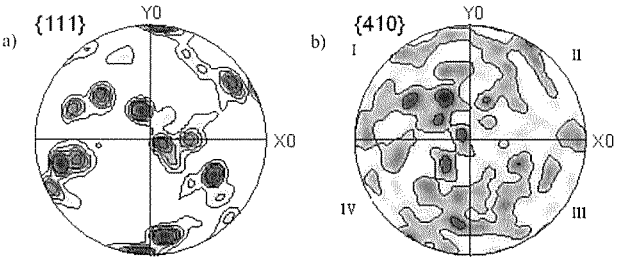

Fig. 10. Pole figures of the α (a) and σ (b) grains for {111} and {410} plane, respectively, EBSD/SEM

The IPF revealed (Fig. 11) that the main [323], [231] peaks of the α phase and the [531] peak of σ phase show a good agreement with the X-ray analysis data.

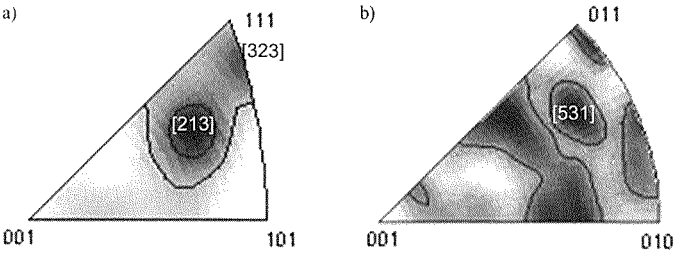

Fig. 11. Inverse pole figure of the α (a) and σ (b) grains for the Z direction, EBSD/SEM

3.5. Crystallographic orientations of the α and σ phases calculated from CBED/TEM measurements

The same cross-section was analyzed by use of CBED/TEM facilities. The scheme of sample axis orientation was also in that case the same as in the X-ray analysis. Phase map of the examined area ($0.05 \cdot 10^{-3}$ mm^2) was presented in Fig. 12.

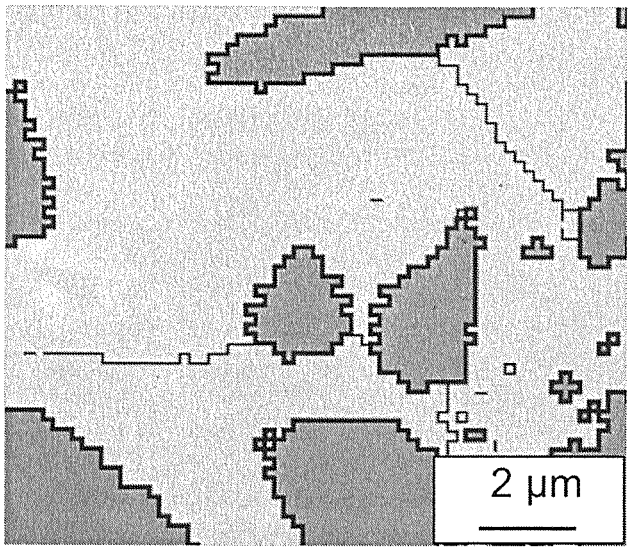

Fig. 12. Phase map of longitudinal section from the bottom of the sample deformed at 800°C. Light grey color corresponds to the α phase, the dark grey – to the σ phase, CBED/TEM

The PF (Fig. 13) and the IPF (Fig. 14) showed that the α grains orientations was close to orientations calculated from the EBSD/SEM measurements while the main peaks from several σ grains in the PF and in the IPF was in a good agreement with the X-ray analysis data.

There is a possibility to define the correlation orientation of different phases in neighbouring grains and the disorientations of particular phases based on EBSD/SEM and CBED/TEM measurements. That will be the next step in the author's research work.

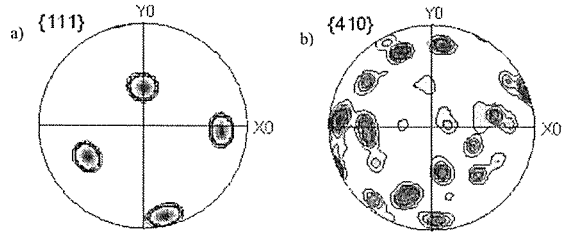

Fig. 13. Pole figures of the α (a) and σ (b) grains for {111} and {410} plane, respectively, CBED/TEM

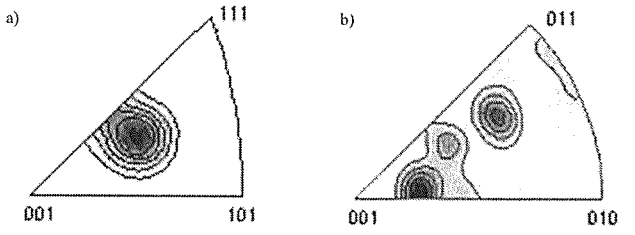

Fig. 14. Inverse pole figure of the α (a) and σ (b) grains for Z direction, CBED/TEM

Received: 3 December 2007.

4. Conclusions

1. Intensive deformation by complex loading resulted in precipitation of the σ phase. Maximum precipitation of the σ phase was observed at 800°C.
2. Orientation distribution of the α phase depended weakly on deformation temperature. For each temperature crystallographic directions [213], [114] of the α phase were parallel to the deformation axis.
3. According to the pole figure obtained by use of X-ray analysis, texture of the α grains was random contrary to the more distinct σ phase texture.
4. Orientations measured by EBSD/SEM, CBED/TEM is scattered around texture components established by X-ray analysis. Some discrepancy of the results is probably the consequence of different sizes of measured areas.
5. X-ray analysis revealed global texture, whereas the data from EBSD/SEM and CBED/TEM measurements delivered more detailed information about orientations and correlations between different phases.

REFERENCES

[1] V. V. Sergeev, T. I. Bulygina, Magnitotverdye Materially (in Russian), Moscow: Energiya (1980).
[2] A. I. Miljaev, Dissertation, Moskva: Institute of Metallurgy and Materials Science (2004).
[3] Ju. K. Kovneristyj, S. P. Efimenko, G. F. Korznikova, A. I. Miljaev, Metalovedenie i termicheskaja obrabotka metallov (in Russian) **5**, 15-17 (2004).
[4] G. F. Korznikova, N. I. Noskova, A. V. Korneva, A. V. Korznikov, Physics of Met. and Metallogr. **98**, 119-127 (2004).
[5] R. Z. Valiev, I. V. Aleksandrov, R. K. Islamgaleev, Prog. Mater. Sci. **46**, p.103 (2000).
[6] H. Gleiter, Nanostructured materials: Basic Concept and Microstructure, Acta Mater. **48**, 1-29 (2000).
[7] M. V. Degtyrev, T. I. Chashuhina, L. M. Voronova, V. P. Pilyugin, Physics of Met. and Metallogr. **90**, 83-90 (2000).